Deciphering the Therapeutic, Larvicidal, and Chemical Pollutant Degrading Properties of Leaves-mediated Silver Nanoparticles Obtained from *Alpinia purpurata*

Manikandan Vani Raju,[a] Meenakshi Kaniyur Chandrasekaran,[a] Meenakshi Sundari Rajendran,[a] Gopalakrishnan Velliyur Kanniappan,[b] Rathi Muthaiyan Ahalliya,[a,*] Guru Kumar Dugganaboyana,[c] Mikhlid H. Almutairi,[d] Bader O. Almutairi,[d] Ameer Khusro,[e] and Ponnuswamy Vijayaraghavan [f]

The aim of the study was to synthesize silver nanoparticles (AgNPs) from *Alpinia purpurata* leaves and evaluate their cytotoxic, antimicrobial, antibiofilm, dye degradation, and larvicidal potentials. The synthesized AgNPs were characterized using ultraviolet-visible spectroscopy, Fourier transform infrared, and high-resolution transmission electron microscopy, which confirmed AgNPs synthesis and revealed nanoparticle size (10 to 30 nm) and the presence of silver. Cytotoxicity tests showed IC_{50} values of 4.59 ± 0.6 µg/mL in A549 cells and 3.48 ± 0.4 µg/mL in PA1 cells, inducing apoptosis and DNA fragmentation. Flow cytometry revealed cell cycle arrest at G0-G1 phase. AgNPs exhibited significant antimicrobial activity, with maximum inhibition zones against *K. pneumoniae* (23 ± 2 mm) and *F. oxysporum* (17 ± 2 mm), and minimum inhibitory concentration (MIC) values ranging from 12.5 ± 0.25 to 75 ± 2.5 µg/mL. They also reduced bacterial and fungal biomass and showed antibiofilm effects. Photocatalytic activity degraded methylene blue dye by 88.4 ± 1.4% in 60 minutes. Larvicidal activity resulted in 100% mortality of *A. aegypti* larvae after 48 hours exposure to AgNPs (10 mg/L), additionally reducing chemical oxygen demand (55.1 ± 2.1% to 63.8 ± 1.5%) and microbial load in wastewater (2.5 to 10 ppm).

DOI: 10.15376/biores.19.2.3328-3352

Keywords: Alpinia purpurata; AgNPs; Cytotoxicity; Antimicrobial; Larvicidal; Photocatalytic activity

Contact information: a: Department of Biochemistry, Karpagam Academy of Higher Education, Coimbatore, Tamil Nadu, India; b: Centre for Plant Tissue Culture and Central Instrumentation Facility, Karpagam Academy of Higher Education, Coimbatore, Tamil Nadu, India; c: Division of Biochemistry, School of Life Sciences, JSS Academy of Higher Education and Research, Mysore, Karnataka, India; d: Department of Zoology, College of Science, King Saud University, P.O. Box 2455, Riyadh 11451, Riyadh, Saudi Arabia; e: Department of Research Analytics, Saveetha Dental College and Hospitals, Saveetha Institute of Medical and Technical Sciences, Saveetha University, Chennai – 600077, India; f: Bioprocess Engineering Division, Smykon Biotech, Kanniyakumari, India;
** Corresponding author: rathiajith@gmail.com*

INTRODUCTION

At present, cancer stands as one of the prominent causes of global mortality, accounting for over 10 million deaths annually. Among diversified forms of cancer, lung cancer is one of the most commonly diagnosed forms of cancer worldwide, which is responsible for the maximum number of cancer-linked fatalities. It is estimated that around 2 million new cases arise each year, resulting in approximately 1.76 million deaths annually. In 2022, the estimated number of lung cancer cases reached 10,3371, securing its

place among the top five prevalent cancer types for both men and women. The overall cancer estimates in India have shown a 5% increment, from 1,392,179 cases in 2020 to 1,461,427 cases in 2022 (Sathishkumar *et al*. 2023).

Although there are disparate reasons for the increasing cases of lung cancer, tobacco usage in our society is the prime cause. According to the data, smokers have a 15 to 30 times greater chance of acquiring lung cancer than non-smokers. Similarly, ovarian cancer ranked as the third most prevalent gynecological cancer worldwide in 2020. Ovarian carcinoma, constituting more than 90% of all cases of ovarian cancer, presents as the most frequent type. It often gets detected in its advanced stages, rendering it the deadliest among gynecological cancers. Generally, its prognosis is low, and over the past five years, it reflected only 17% survival rate for individuals in the advanced stages. As a result, it becomes crucial to know the causes and risk factors of ovarian cancer to prevent the onset of this illness (Huang *et al*. 2022). Caspases, a family of 15 cysteine proteases, play crucial roles in programmed cell death and inflammation. Among these, caspase-3 serves as a typical executor of apoptosis. Its activation by initiator caspases such as caspase-8 or caspase-9 leads to the cleavage of various vital proteins in the cell, ultimately inducing apoptosis. Many treatments for cancer, such as cytotoxic drugs, radiotherapy, or immunotherapy, induce tumor cell death by triggering caspase-3 activation. So, numerous researchers utilize caspase-3 activation as an indicator of the effectiveness of cancer therapies (Zhou *et al*. 2018).

Nanotechnology has emerged as a revolutionary tool in the field of drug delivery, with the capacity to transform medication administration and targeting. It greatly improves drug efficacy while modifying the adverse effects (Anjum *et al*. 2021). Green synthesis of nanoparticles plays a crucial role in the field of medicine, as it provides safer and more efficient approaches for the therodiagnostic purpose of any disease. With respect to the other methods of synthesis, green synthesis method is steadily gaining popularity and recognition, particularly because of its sustainability, environmental awareness, and safety (Aboyewa *et al*. 2021). Using hot water as the extraction solvent can be advantageous. Primarily, hot water extraction is considered safer and more environmentally friendly compared to organic solvents including ethyl alcohol, which may pose health and safety risks and require additional processing steps for solvent removal. Additionally, hot water extraction is efficient in extracting a wide range of compounds, including polar and heat-stable molecules such as polysaccharides, proteins, and some alkaloids, commonly found in plant materials. Moreover, hot water extraction is relatively simple, cost-effective, and easily scalable, making it a practical choice for large-scale extraction processes. Overall, these factors contribute to the preference for using hot water as the extraction solvent in various studies (Castro-Puyana *et al*. 2017). Biosynthesized silver nanoparticles hold potential as cancer therapeutics, especially against lung cancer. While cytotoxic assays have been the main approach to studying their effects, biologically synthesized AgNPs have also been found to disrupt the cell cycle, influence signaling pathways, induce cell death, and enhance the production of intracellular molecules (Mejia-Mendez *et al*. 2023). Silver nanoparticles are an excellent vehicle in carrying or encapsulating plant-derived therapeutic agents, such as antioxidants or anti-inflammatory drugs, which enhances their uptake and efficacy in the treatment of non-communicable diseases. Due to its unique characteristics and extensive applications, AgNPs are playing a significant role in oncological research (Li *et al*. 2020). AgNPs have the ability to impair the mitochondrial process in cancer cells, which causes energy depletion and cell death. One important mechanism behind their anticancer effect may be the disturbance of mitochondrial

function. AgNPs can cause cell death by activating apoptotic pathways in cancer cells *via* several routes. In the study reported by Artiukh *et al*. (2022), it was observed that in noncancerous cell lines, the cellular parameters remained similar to those of the untreated control cells. A plethora of studies are under investigation to reduce cytotoxicity and stop the development of cancer cells (Hashem *et al*. 2022). A critical checkpoint in the apoptotic cascade, *i.e.*, caspase 3 activation, ensures the ordered and regulated death of cells. This process is necessary for a number of physiological and pathological circumstances, such as tissue growth, repair, and the body's response to cell damage. Because of its pivotal function in apoptosis, caspase 3 is a topic of considerable interest in both fundamental cell biology and clinical research for conditions like cancer (Takáč *et al*. 2023).

Alpinia purpurata, commonly referred to as red ginger or ostrich plume, is a tropical flowering plant native to Malaysia and the Pacific Islands. Its cultivation is primarily for the sake of its ornamental and captivating flowers. This perennial, herbaceous plant has the potential to grow up to a towering height of 10 ft (approximately 3 m) (Arul Raj *et al.* 2012). In ancient times, it found utility in addressing a variety of health concerns, including digestive ailments and skin irritations (Anusooriya *et al.* 2022).

Considering the wide-ranging applications of nanoparticles, it is hypothesized that AgNPs synthesized using *A. purpurata* leaves will exhibit cytotoxic activity against A549 and PA1 cancer cell lines, inducing apoptosis in cancer cells by activating Caspase 3. Also, the nanoparticles are evaluated for antimicrobial, antibiofilm, dye degradation, and larvicidal potentialities.

EXPERIMENTAL

Materials and Methods

Plant collection and extract preparation

A specimen of *A. purpurata* was collected from Kanyakumari, Tamil Nadu, India, and its authenticity was confirmed by Dr. G.V.S. Murthy, Director, Botanical Survey of India, TNAU campus, Coimbatore, India. To preserve it for future reference, a voucher specimen was archived in the laboratory under the code - BSI/SC/5/23/10-11/Tech. The leaves of *A. purpurata* were collected, dried in the shade, and then ground into a fine powder. This powder (500 g) was subjected to extraction with water in a 2:10 (weight-to volume) ratio using a Soxhlet apparatus for 72 h. The resulting extract was further processed by a complete drying process using a rotary flash evaporator of Buchi type for further purposes.

Qualitative phytochemical screening

The desiccated aqueous extract was diluted with water and subjected to a qualitative phytochemical analysis for confirming the presence of alkaloids, flavonoids, tannins, phenols, saponins, terpenoids, steroids, and glycosides (Thotathil *et al.* 2022).

Test for alkaloids

The presence of a brownish-red precipitate after adding six drops of Dragendorff reagent to 1 mL of plant extract and 1 mL of 1% HCl indicates the presence of alkaloids.

Test for steroids

A blue-green ring that forms after adding equal parts of chloroform and acetic anhydride to 1.0 mL of plant extract indicates the presence of steroids.

Flavonoids

To 5 mL of diluted ammonia solution, 1.0 mL of concentrated sulphuric acid, and 5 mL of plant extract were added. Yellow colour formation indicates the presence of flavonoids.

Tannins

A blue-black precipitate formed after adding a few drops of ferric chloride to 1.0 mL of plant extract showed that tannins were present.

Reducing Sugars

A few drops of Fehlings solutions A and B were added to 1.0 mL of plant extract orange-red precipitate, confirming the presence of reducing sugars.

Cardiac glycosides

A 2 mL of sample 1 mL of glacial acetic acid was prepared containing a few drops of $FeCl_3$. Conc.H_2SO_4 was added to the above mixture, giving a green-blue colour and indicating the positive results for the presence of cardiac glycosides.

Saponins

To 1.0 mL of plant extract, 5 mL of distilled water was added, and the mixture was violently agitated for 2 minutes. The development of stable foam is a sign that saponins are present.

Terpenoids

2 mL of chloroform and 3 mL of concentrated sulphuric acid were added to 1.0 mL of plant extract. The presence of terpenoids was confirmed by reddish-brown colour development.

Green synthesis of AgNPs

The aqueous extract of *A. purpurata* was mixed with the freshly prepared silver nitrate solution in a 1:1 ratio and kept at room temperature undisturbed. After 24 h, a noticeable brownish coloration was observed. After this, the mixture was centrifuged at 18,000 rpm for 20 min. The resulting pellet was carefully rinsed with double distilled water and then allowed to air-dry at room temperature for further characterization purposes (Vijay *et al.* 2023).

AgNPs characterization

Ultraviolet-visible (UV-Vis) spectrophotometry (Thermo Fisher Evolution 201; Full Thermo Fisher Scientific Inc., Waltham, MA, USA) analysis was conducted within the wavelength range of 200 to 900 nm. Fourier transform infrared (FT-IR) analysis was performed using a Shimatzu (IRTracer-100; Shimadzu Corporation, Kyoto, Japan) spectrometer, covering the spectral range 4000 to 400 cm^{-1}. High-resolution transmission electron microscopy (HR-TEM) (JEOL JEM 2100 High Resolution Transmission Electron Microscope; JEOL Ltd., Akishima, Japan) analysis provided qualitative measurements of

the synthesized nanoparticles, including particle size, distribution, and morphology. Energy dispersive microanalysis (EDX) techniques were used to verify the presence of silver as well as other metal elements within the synthesized nanoparticles (JEOL JEM 2100 High Resolution Transmission Electron Microscope; JEOL Ltd., Akishima, Japan).

Cytotoxic activity

Lung cancer cell line (A549) and ovarian cancer cell line (PA1) cells were purchased from the National Center for Cell Science, Pune (India). The cytotoxicity of AgNPs on both A549 and PA1 cells was evaluated using the MTT assay (Mosmann 1983). For this assay, cells were seeded at a density of 1×10^5 cells per well in 96-well plates, with each well containing 0.2 mL of medium. These plates were then placed in a 5% CO_2 environment for 72 h. After the initial incubation, varying concentrations of AgNPs, each with 0.1% dimethyl sulfoxide (DMSO), were introduced into the wells and incubated for an additional 48 h in the presence of 5% CO_2. Cell images were captured using an inverted microscope (IX53; Olympus Corporation, Shinjuku City, Japan) at 40X magnification, and photographs were taken. Following the removal of the sample solutions, a solution containing 3-(4,5-dimethyl-2-thiazolyl)-2,5-diphenyl-tetrazolium bromide (MTT) at a concentration of 5 mg/mL in phosphate-buffered saline (PBS) solution (20 µL/well) was added. After 4 h, 1 mL of DMSO was added to each well. The quantification of viable cells was achieved by measuring the absorbance at 540 nm. Subsequently, measurements were conducted, and the concentration required to achieve a 50% inhibition of cell viability (IC_{50}) was determined through graphical analysis.

Flow cytometry

Initially, the cells were cultured in T25 or T75 culture flasks. Upon reaching confluence, the cells were transferred to 6-well adherent culture plates. After 24 h, the cells were treated with the IC_{50} concentration of AgNPs for an additional 24 h. To harvest the cells, trypsinization was carried out using a trypsin (0.05%)-EDTA (0.54 mM) solution. The cells were then washed thoroughly with culture media through vortexing, followed by centrifugation at 1200 rpm for 5 min. This was followed by a wash with PBS and centrifugation at 1200 rpm for 5 min. The supernatant was discarded, and the pellet was resuspended in 300 µL of PBS within a falcon tube. Subsequently, 700 µL of ice-cold 100% ethanol was added to fix the cells. The ethanol-fixed cells were washed twice with PBS, and the supernatant was removed. Triton X-100 (556 µL at 0.5%), containing RNase (20 µL at 0.1 mg/mL), was added and incubated for 1 h. After that, 24 µL of propidium iodide (at a concentration of 40 µg/mL) was added and incubated further in the dark for 45 min (Plotnikov *et al*. 2023). The samples were then analyzed using a flow cytometer.

DNA fragmentation analysis

Cancer cells (A549 and PA1) were seeded in 12-well plates and incubated in a 5% CO_2 incubator for 72 h. Subsequently, 1 mL of the respective samples was added to the wells and incubated for 24 h in a 5% CO_2 incubator. After removing the sample solution, 500 µL of TPVG (trypsinization) was added, and the solution was discarded. After this, 1 mL of 1X PBS solution was added to collect the samples for DNA fragmentation analysis (Gad *et al*. 2021).

RT-PCR analysis

Total RNA was extracted for the AgNPs-treated A549 and PA1 cells, as per the manufacturer's guidelines using TRIzol reagent. The concentration of RNA was determined using spectrophotometric method. Subsequently, 1 µg of total RNA was utilized for a reverse transcription reaction. The cDNA was precipitated and amplified using specific primer sequences to ensure efficient and targeted amplification. Primer sets targeting Cas-3 (apoptotic gene) and GAPDH (housekeeping gene) were specifically designed for cDNA amplification (Baharara *et al*. 2015). The primers used for analysis are shown in Table 1.

Table 1. Primers Used for RT-PCR Analysis

No	Gene	Forward	Reverse
1	Cas- 3	5'-AGGGGTCATTTATGGGACA- 3'	5'-TACACGGGATCTGTTTCTTTG-3'
2	GAPDH	5'-CCATGTTCGTCATGGGTGTGAACCA-3'	5'-GCCACTAGAGGCAGGGATGATGTTC-3'

Microorganisms used and culture preparation

Bacteria [*Enterococcus faecalis* (MTCC 439), *Bacillus subtilis* (MTCC 482), *Bacillus coagulans* (MTCC 492), *Enterobacter cloacae* (MTCC 509), *Pseudomonas aeruginosa* (MTCC51034), *Klebsiella pneumoniae* (MTCC 432), and *Staphylococcus aureus* (MTCC902)], and fungi [*Aspergillus niger* (MTCC404), *Fusarium oxysporum* (MTCC 2087), *Rhizopus microsporus* (MTCC 1250), *Rhizopus oryzae* (MTCC262), and *Penicillium chrysogenum* (MTCC 947)] used in this study were obtained from the Microbial Type Culture Collection and Gene Bank, Chandigarh, India.

Antimicrobial activities of AgNPs

The bacterial cultures were cultivated in 250-mL Erlenmeyer flasks containing 100 mL of Mueller Hinton broth (MHB) (Himedia, Mumbai, India) and incubated at 37 °C in a rotary shaker incubator for 24 h. The cultures were maintained to reach 0.1 OD at 600 nm, and mid-log phase bacterial cultures were used for antibacterial activity. The fungal strains were cultivated on Sabouraud Dextrose Agar (SDA) (Himedia, Mumbai, India) for 5 days at 28 °C. After 5 days of incubation, 10 mL of ice-cold double distilled water was added, and the spore suspension was used for antifungal activity.

Disc diffusion assay

The antibacterial activity of the extract was initially screened against the selected bacterial pathogens by disk diffusion method. The bacterial cultures were spread on sterile MHA medium using a sterile cotton swab. The sterile blank disk was loaded with 20 µL of NPs and dried. It was further placed on the MHA plates and incubated at 37 °C for 24 h. After 24 h, the zone of inhibition was measured.

Minimum Inhibitory Concentration (MIC)

The minimum inhibitory concentration of AgNPs was tested as described previously. The AgNPs were serially diluted in 2% DMSO, and the initial AgNPs concentration was 0.25 mg/mL. The test solution was serially diluted twofold. The experiment was performed on a microtiter plate and inoculated with 20 µL of bacteria (10^7 CFU/mL). The microtiter plates were incubated at 37 ºC for bacteria, and the visible growth was examined after 24 h. Streptomycin was used as the positive control. The MIC value of the AgNPs was calculated as the absolute lowest amount of the NPs completely inhibiting the visible growth of the test bacteria in microtiter plates.

Fungal biomass inhibitory effect

The fungal biomass inhibitory property of AgNPs was analyzed as described previously. Briefly, 100 mL of potato dextrose broth (PDB) was mixed with 0.5 mg/mL of AgNPs and inoculated with 0.5 mL of fungus (1×10^7 CFU/mL). The flasks were incubated for 5 days at 28 °C. After 5 days of incubation, fungal hyphae were filtered using a Whatman number 1 filter paper. The fungal biomass was determined, and the result was compared with the positive control.

Antibiofilm activity of AgNPs

The antibiofilm activity of AgNPs was evaluated at 1/2, 1/4, and 1/8 MIC values of the AgNPs. The antibiofilm assay was performed using crystal violet staining method. Briefly, the selected bacterial strains were cultured in a microtiter plate containing 400 µL of sterile MHB medium, inoculated with 20 µL of culture medium, and incubated at 37 °C for 24 h. In the microtiter plates, particular concentrations of AgNPs were supplemented. After 24 h, the floating non-adherent bacterial cells were completely removed and air dried for 30 min. After 30 min, the plates were dried, and the wells were stained with crystal violet and incubated in the dark for 10 min. Then, the excess stain was removed and washed with sterile, double-distilled water. The plate was air dried, 250 µL of ethanol (90%) was added, and the absorbance of the sample was measured at 620 nm against the reagent blank. The percentage optical density of the microtiter plate wells treated with AgNPs was compared with the control.

Photocatalytic activity of AgNPs on methylene blue

Methylene blue (MB) was prepared at a concentration of 10 ppm in the double-distilled water. Two mL of MB was mixed with 0.5 mL of AgNPs solution (10 ppm) in very clean glassware. The photocatalytic activity was regularly monitored at 660 nm for 60 min. The dye degradation potentials of NPs were calculated using Eq. 1,

$$\text{Dye degradation (\%)} = (1 - A_t/A_0) \quad (1)$$

where A_t is the absorbance after time t (min) and A_o is the initial absorbance.

Larvicidal activity of AgNPs

Third instar *Aedes aegypti* (n = 48) larvae were maintained in a glass beaker. To the beakers, 100 mL of tap water was added, and different concentrations (2.5 to 10 mg/L) of green synthesized AgNPs were fixed. To the control group, only tap water was added. A complete randomized experimental trial was performed. The number of dead larvae was counted after 24 and 48 h of exposure and percentage mortality was registered.

Chemical Oxygen Demand (COD) and bacterial load determination in municipal wastewater

The COD analysis of municipal wastewater (n = 4) before and after AgNPs treatment was performed using colorimetric method. Aliquots of a 10 mL sample were collected before and after AgNPs treatment. The COD analysis was performed without any sediment particles. The serial dilution method was used for the determination of total bacteria in the treated wastewater.

Statistical Analysis

GRAPHPAD PRISM 9 (GraphPad Software In, PRISM 9, La Jolla, CA, USA) was used for the statistical analysis. Experiments were performed in triplicate. The average standard deviation (SD) of the used triplicates was used to reflect the outcomes of each experiment. One-way analysis of variance (ANOVA) (Dunnett's test) was used to achieve the examination of variance and significant variations between the means with $p < 0.05$.

RESULTS AND DISCUSSION

Qualitative Phytochemical Screening

The aqueous extract of *A. purpurata* contains a spectrum of valuable phytochemicals, including alkaloids, tannins, phenolic compounds, flavonoids, steroids, and terpenoids (Table 2). These phytochemicals are organic compounds naturally found in plants, each with their unique properties and potential health benefits. The presence of various compounds in the extract, such as alkaloids, proteins, enzymes, amino acids, alcoholic compounds, and polysaccharides, indicates a complex mixture with potential reducing properties for silver ions (Mittal *et al*. 2013). Alkaloids and tannins are recognized for their potent antioxidant capabilities and potential medicinal uses. Flavonoids are known for their strong antioxidant and anti-inflammatory properties, making them the phytoconstituents of great interest in health and nutrition (Ullah *et al*. 2020). Steroids, a diverse group of compounds, play dynamic roles in various biological processes and are crucial in physiological functions (Adhya *et al*. 2018). Additionally, terpenoids, with their vast diversity, exhibit a wide range of pharmacological properties and have been utilized in traditional medicine for their potential health advantages.

Table 2. Qualitative Phytochemical Screening of *A. purpurata*

S. No	Phytochemicals	Aqueous Extract
1	Alkaloids	+
2	Saponin	-
3	Tannin and phenolic compounds	+
4	Flavonoids	+
5	Steroids	+
6	Cardiac glycosides	-
7	Oils and fats	-
8	Terpenoids	+
9	Amino acids and proteins	-
10	Carbohydrates	-

Presence (+), Absence (-)

In the realm of cancer treatment, specific alkaloids have revealed formidable cytotoxic effects on cancer cells. They disrupt vital cellular mechanisms, such as DNA replication, cell cycle progression, and protein synthesis. Ultimately, this disruption triggers apoptosis within cancer cells. Also, alkaloids have been noted for their ability to delay angiogenesis (an essential process for tumor advancement and metastasis by inhibiting the growth of new blood vessels) (Khan *et al*. 2022).

AgNPs Synthesis

Synthesis of AgNPs was confirmed by observing the change in color of the mixture from orange to brown (Fig. 1). This transformation was a result of the bio-reduction of silver nitrate by the phytochemicals present in the plant extract. Color transformation was regularly observed, and a visible change was noticed after about 3 to 4 h. This shift to a deeper and darker color is attributed to the surface plasmon resonance, a size-dependent trait of nanoparticles. Surface plasmon resonance plays a crucial role in the comprehensive investigation and design process of new nanoparticles for biomedical applications (De Macedo *et al*. 2022). The intensity of the color change reflects effective bio-reduction of silver ions, resulting in a significant yield of silver nanoparticles within 24 h (Anandalakshmi *et al*. 2015).

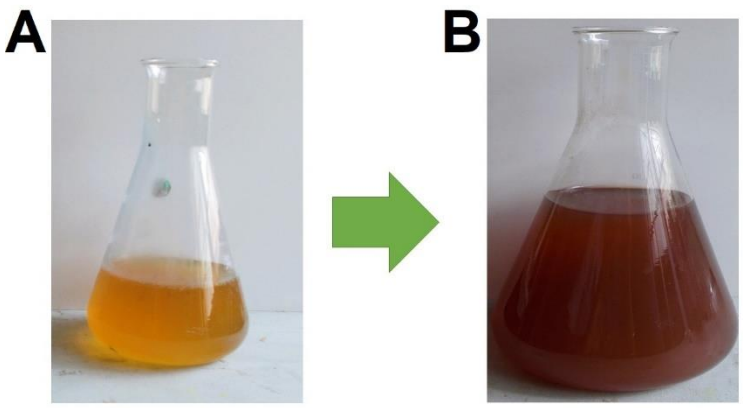

Fig. 1. Color changes during the synthesis of AgNPs **(A)** Plant extract and **(B)** Synthesized AgNPs

Characterization of AgNPs

UV-Vis spectral analysis

Upon analyzing the spectrum of the synthesized nanoparticles, a prominent absorbance peak at 420 nm was observed (Fig. 2A), which is a characteristic of surface plasmon resonance for green-synthesized nanoparticles (Kumar *et al*. 2023). An extraordinary optical property of AgNPs lies in their strong interaction with specific light wavelengths. This interaction varies based on the size and morphology of the synthesized nanoparticles, giving rise to a spectrum of colors, spanning from orange to brown. In this study, the peak exhibited a broad spectrum extending from 300 to 600 nm, strongly indicating the presence of AgNPs in the sample solution due to surface plasmon resonance. The obtained results closely resembled those reported in previous study (Kumar *et al*. 2023).

FT-IR analysis

AgNPs displayed distinct absorbance bands in the infrared spectrum. Notably, a strong absorbance band was observed at approximately 3410.2 cm^{-1}, which can be accredited to the presence of bonded O-H groups. Another absorbance band was noted at approximately 16249.1 cm^{-1}, indicating the presence of C=C groups. Also, absorbance bands were identified at around 1388.8 cm^{-1} and 1112.9 cm^{-1}, corresponding to the presence of C-N and C-O groups (Fig. 2B). The carbonyl group within amino acid residues demonstrates a healthy affinity for silver, implying the development of protective layers composed of AgNPs. These layers act as effective capping mediators, preventing agglomeration and conferring stability to the medium. This further validates the role of phytocompounds, not only in reducing silver ions but also in stabilizing the resultant nanoparticles (Zuhrotun *et al*. 2023).

HR-TEM with EDX

To ascertain the structural morphology, a detailed TEM analysis was performed. The TEM micrographs distinctly displayed AgNPs with a particle size ranging between 10 and 30 nm (Fig. 2C). This technique stands as a potent tool for precise characterization of the size and shape of nanoparticles. The selected area electron diffraction pattern (SAED) of the synthesized AgNPs showcased prominent and well-defined rings (Fig. 2D). The nanoscale characterization through TEM further gave evidence of successful nanoparticle synthesis from the extract. For a deeper understanding, an EDX micro-analysis was conducted, involving the study of energy and intensity distribution of X-ray signals originating from the electron beam interacting with the specimen. The resulting peaks in the EDX analysis are graphically shown in Fig. 2E. These spectra conclusively validate the presence of silver (Ag) within the synthesized AgNPs. Additionally, there were distinct peaks corresponding to other metallic elements, including copper (Cu). These elements point to the existence of capping organic agents firmly bound to the surface of the AgNPs (Abdulazeem *et al*. 2023). The rings represent the crystallographic planes characteristic within the AgNPs, offering critical insights into their crystalline structure. The distinct arrangement and characteristics of these rings within the diffraction pattern provide a window into the orientation and spatial organization of the nanoparticles, elevating our understanding of their properties and potential applications (Mourdikoudis *et al*. 2018).

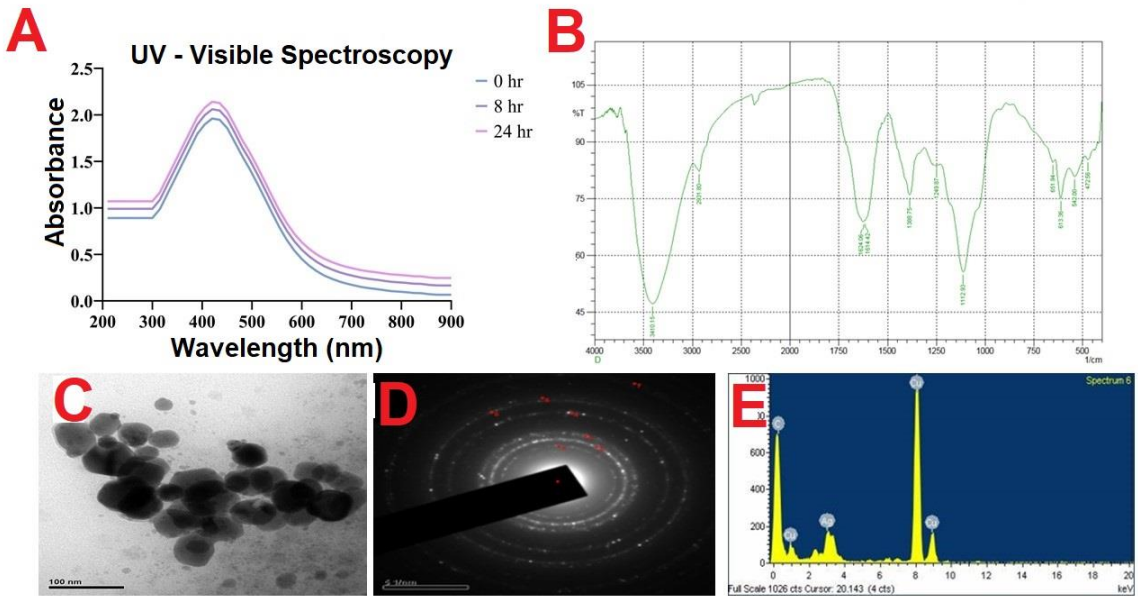

Fig. 2. Characterization of AgNPs: (A) UV-Vis spectra, (B) FT-IR spectrum, (C) HR-TEM image, (D) SAED pattern, and (E) EDX analysis

Cytotoxic Activity

Phase contrast images of A549 and PA1 cells at different concentrations of AgNPs represented significant alterations in the cellular morphology, mainly cell detachment and cellular shrinkage, indicating a notable reduction in cell viability. The inhibition of cell growth ultimately led to cell death. The study unequivocally demonstrates that the cytotoxic activity of AgNPs is a dose-dependent process (Fig. 3A). The IC_{50} values for AgNPs were calculated as 3.48 ± 0.4 µg/mL for PA1 cells (Fig. 3B) and 4.59 ± 0.6 µg/mL for A549 cells (Fig. 3C). In a previously reported study, AgNP at a concentration of 2.5 µg/mL showed 80% viability of healthy cells, whereas the viability of cancer cells was less than 50%. This significant difference underscores the potential selectivity of AgNPs in targeting and affecting cancer cells, while exhibiting relatively lower impact on healthy cells, which is a critical aspect for considering their application in cancer therapeutics (Artiukh *et al*. 2022).

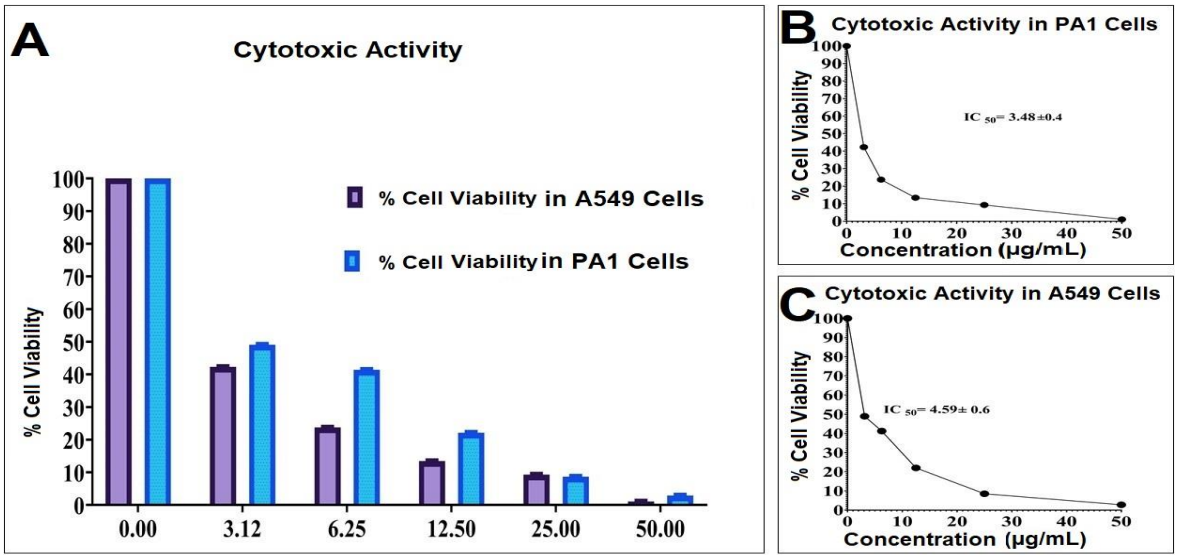

Fig. 3. (A) Cytotoxic activity against A549 and PA1 cells, **(B)** IC_{50} determination against PA1 cells, and **(C)** IC_{50} determination against A549 cells

Flow cytometry

This study confirmed that exposure of A549 cells and PA1 cells to 4.59 ± 0.6 and 3.48 ± 0.4 µg/mL of AgNPs led to 25.8% and 54.9% apoptosis (Fig. 4 D, E, and F). In contrast, the control group exhibited a remarkably high percentage of viable cells (99.86% in A549 and 98.28% in PA1 cells). The flow cytometry analysis results are visually presented in Fig. 4 J, K, and L. In the control A549 cells, the R5 range signifies the presence of cell viability in the G0-G1 phase, with a recorded viability of 99.86%. Conversely, the treated A549 cells exhibited cell death, as indicated by the R5 range at 76.4%, and the viable cells in the G0-G1 phase at 25.8%. Moving to the control PA1, the R5 range also indicated the occurrence of cell viability in the G0-G1 phase, with a measured viability of 98.3%. However, the treated PA1 displayed cell death, marked by the R5 range at 47.6%, and the highest percentage of viable cells in the G0-G1 phase at 54.9%.

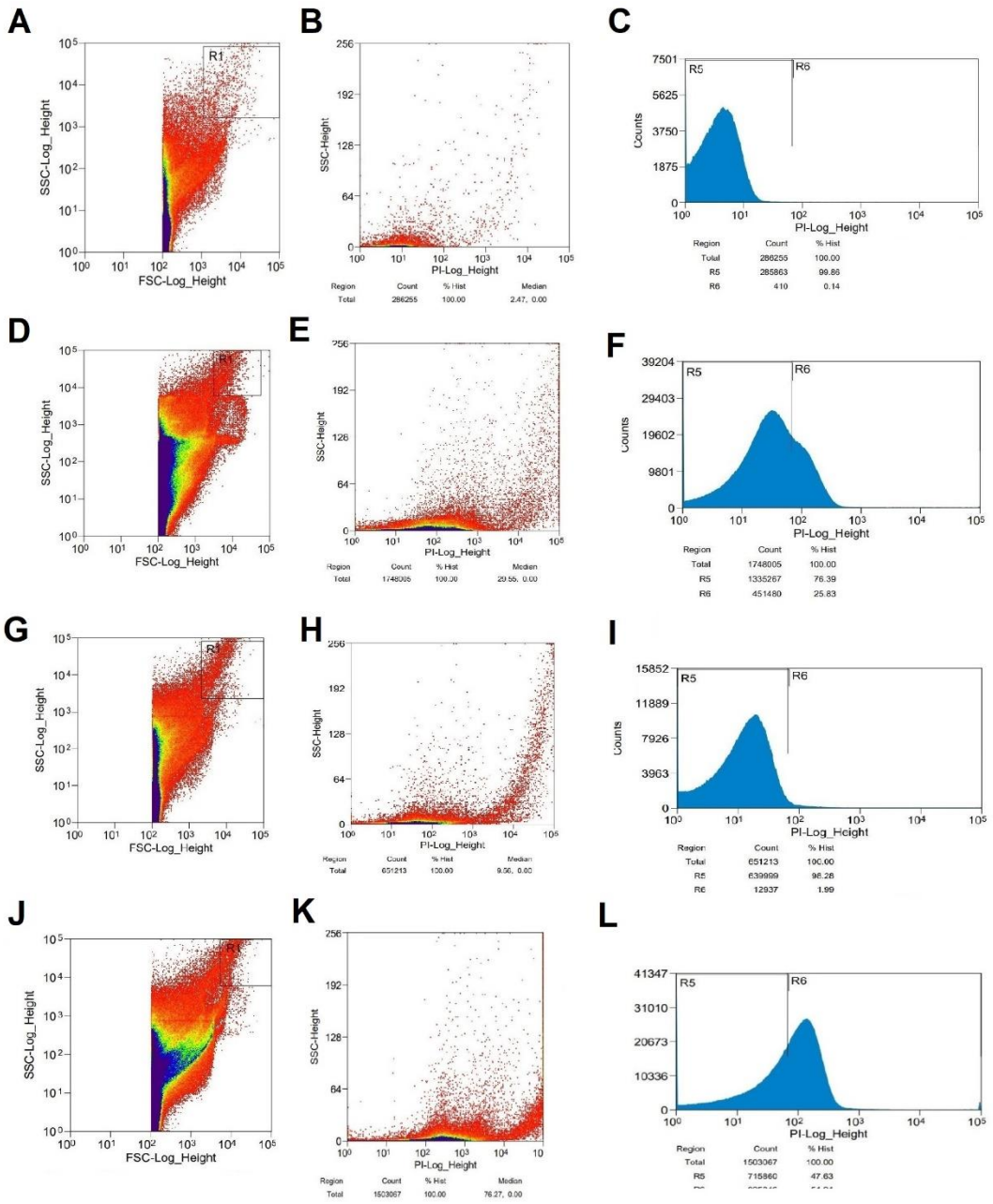

Fig. 4. (A), (B), and **(C)** Flow cytometry graph of control A549 cells; **(D), (E),** and **(F)** Flow cytometry graph of treated A549 cells; **(G), (H),** and **(I)** Flow cytometry graph of control PA1 cells; **(J), (K),** and **(L)** Flow cytometry graph of treated PA1 cells

The conflicting results observed in this study strongly suggest that the involvement of additional parameters that influence nanoparticle-mediated cell death. These variations in outcomes may arise from complex interactions influenced by factors, such as nanoparticle size, concentration, exposure duration, cell type, and the specific biological environment (Mohammadi *et al*. 2021). In the study conducted by Rezazadeh *et al*. (2018), local delivery (aerosol) of chemotherapeutic drugs to the lungs was highlighted as offering numerous advantages for the treatment of lung cancer in comparison to conventional

systemic chemotherapy. The researchers synthesized novel mixed polymeric micelles, comprising tocopheryl succinate-polyethylene glycol and loaded them with paclitaxel. Subsequently, the optimized micelles were incorporated into lactose carrier particles using a spray drying technique, resulting in the creation of a colloidal aerosol drug delivery system.

The findings presented in the study conducted by (Lee *et al.* 2011) demonstrated comparable outcomes, indicating that silver nanoparticles exhibit similar efficacy in cell arrest. The contradictory outcomes observed in this investigation strongly indicate the potential influence of supplementary factors affecting nanoparticle-induced cell death. Apoptosis induced in the cells treated with AgNPs resulted in a decrease in the proportion of cells in the G0/G1 phase and an elevation in the proportion of cells in the G2/M phase. This shift indicates cell cycle arrest at the G2/M phase.

DNA fragmentation analysis

To evaluate the effect of the synthesized AgNPs on DNA damage, the A549 and PA1 cell lines were treated with 100 µL of the effective concentration (as determined by the MTT cell viability assay) of AgNPs for 24 h. The results vividly demonstrated that AgNPs induced a prominent increase in cell death by causing fragmentation of nuclear DNA in both A549 and PA1 cells, resulting in a distinct ladder-like pattern. This observation underscores the potential of AgNPs to induce significant cellular changes, particularly in terms of DNA integrity and cell viability. A comparable outcome was substantiated by Chaturvedi *et al*. (2020), wherein cancer cell lines treated with silver nanoparticles exhibited the distinct formation of a DNA ladder pattern. In a previously reported in vivo study, it was observed that high amounts of silver nanoparticles accumulated in the cancerous tissue of solid tumor-bearing mice following intravenous and intratumoral injection of radioactively labeled AgNPs. Although some nanoparticle accumulation was noted in the liver and spleen of the animals, the substantial accumulation in tumor tissue indicates that intravenously administered AgNPs have the capability to effectively reach cancerous tissue (Sakr *et al*. 2018). The study proposed by Gurunathan *et al*. (2013) showed that the exposure to AgNPs prompted the generation of micronuclei. This suggests that nanoparticles, along with reactive oxidative species, instigate DNA damage, thus triggering the activation of p53 and DNA repair-related proteins. This mechanism bears resemblance to the carcinogenesis induced by irradiation.

RT-PCR analysis

Figures 5C and D show Caspase-3 expression due to AgNPs on A549 and PA1 cells. These findings provide compelling evidence regarding the apoptotic potential of silver nanoparticles in human A549 and PA1 cells, highlighting their promising role in inducing apoptosis and potentially inhibiting cancer cell growth. Understanding and analyzing the complex elements are crucial for separating the complex mechanisms that underlie nanoparticle-induced cellular responses and apoptosis. Further research and a comprehensive exploration of these diverse features will not only enhance our understanding of nanoparticle-cell interactions but also refine their potential applications in various biomedical domains. Caspase-3, a protease enzyme, is frequently activated within cells, being a vital component of both intrinsic and extrinsic apoptosis pathways. The intrinsic pathway is initiated by signals originating from within the cell, often prompted by cellular stress or DNA damage. Conversely, the extrinsic pathway is activated by external signals, typically halting from factors in the cellular environment or

neighboring cells. Also, there have been thoughtful efforts to adapt AgNPs, optimizing them for precise targeting of cancer cells. This enhancement aims to enlarge their ability to induce apoptosis by activating caspase-3. Silver nanoparticles possess the capacity to deliver apoptotic signals selectively to cancer cells, prompting caspase-3 activation and enabling regulated cellular death within the tumor. The complex interaction between AgNPs and caspase-3 holds a key role in the progression of precise cancer therapies. Utilizing the capabilities of AgNPs to control caspase-3 activation leads pioneering and efficient approaches in cancer treatment. These strategies prioritize the induction of apoptosis in malignant cells, while minimizing the adverse effect on the healthy cells.

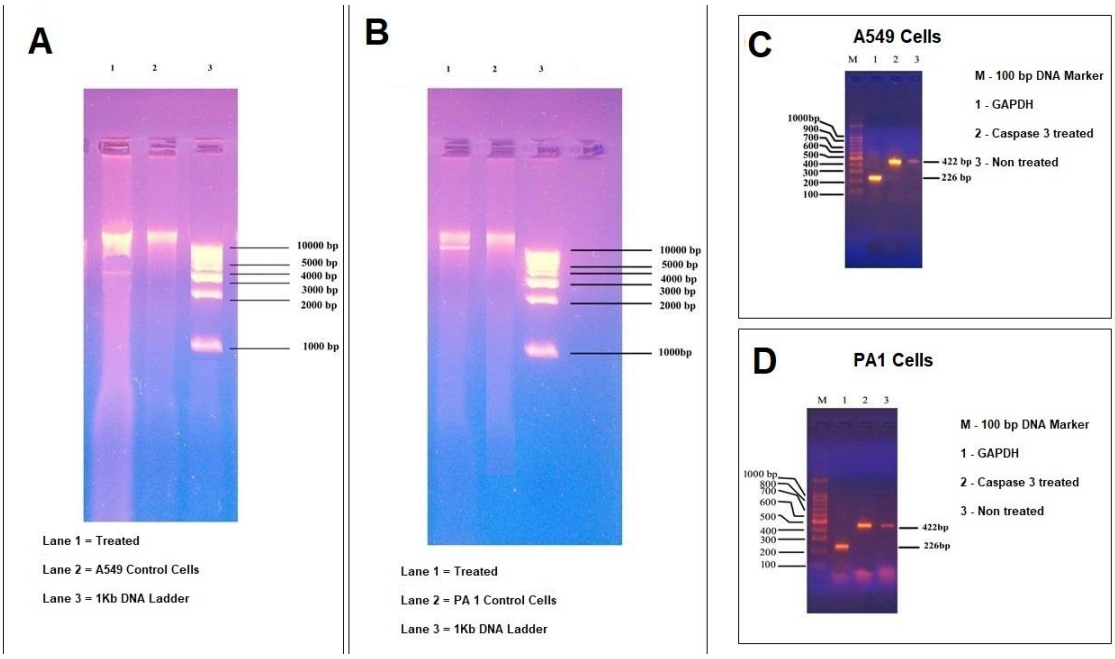

Fig. 5. (A) DNA fragmentation of A549 cells, **(B)** DNA fragmentation of PA1 cells, **(C)** Caspase 3 expression in A549 cells, and **(D)** Caspase 3 expression in PA1 cells

Antibacterial activity of AgNPs

Findings revealed that the AgNPs were effectively suppressing the growth of human bacterial pathogens at different potencies. As illustrated in Fig. 10, AgNPs exhibited the maximum zone of inhibition against *K. pneumoniae* (23 ± 2 mm), followed by *P. aeruginosa* (21 ± 2 mm) and *B. subtilis* (19 ± 2 mm). Moreover, AgNPs exhibited less zone of inhibition against *E. faecalis* (16 ± 1 mm), *S. aureus* (16 ± 1 mm), *B. coagulans* (13 ± 1 mm), and *E. cloacae* (9 ± 0 mm), correspondingly (Fig. 6). In this study, the green-synthesized AgNPs exhibited antimicrobial activities against clinical pathogens. Generally, AgNPs exhibit antimicrobial activity by several cellular mechanisms, including inducing oxidative stress, releasing metal ions, generating reactive oxygen species, causing loss of microbial cell integrity, and damaging proteins and DNA (Al-Wrafy *et al*. 2022).

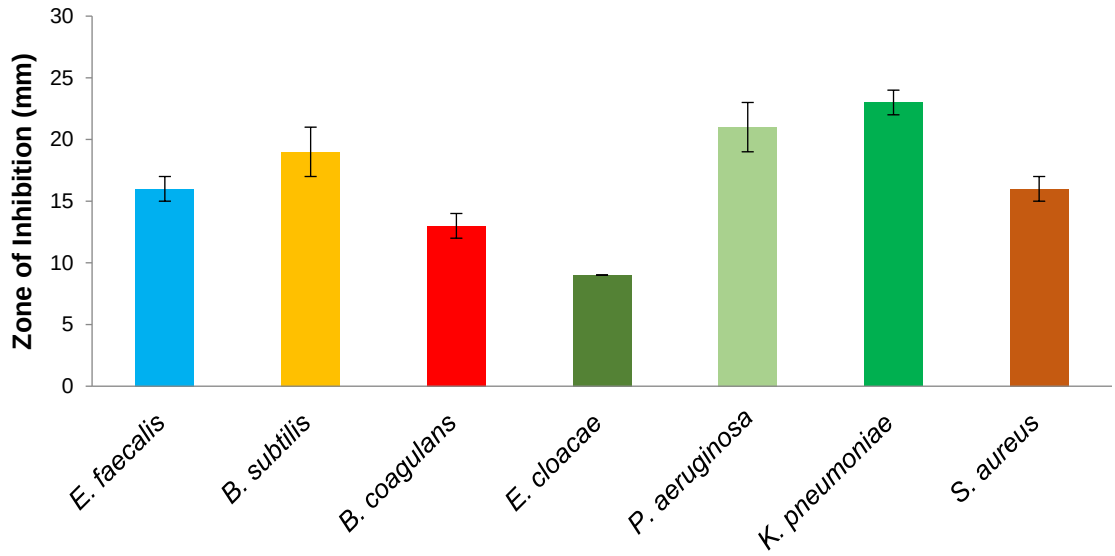

Fig. 6. Antibacterial activity of AgNPs against bacterial pathogens

Antifungal Activity of AgNPs

AgNPs inhibited fungal mycelia growth and exhibited the maximum zone of inhibition against *F. oxysporum* (17 ± 2 mm). The antifungal activity ranged from 9 ± 0 mm to 17 ± 2 mm and the sensitivity varied based on the types of fungi. Two *Rhizopus* strains (*R. microsporus* and *R. oryzae*) were selected for this study and AgNPs showed 10 ± 2 mm and 16 ± 2 mm of zone of inhibition against *R. microsporus* and *R. oryzae*, correspondingly. AgNPs exhibited a < 10 mm zone of inhibition against *A. niger* and *P. chrysogenum* (Fig. 7).

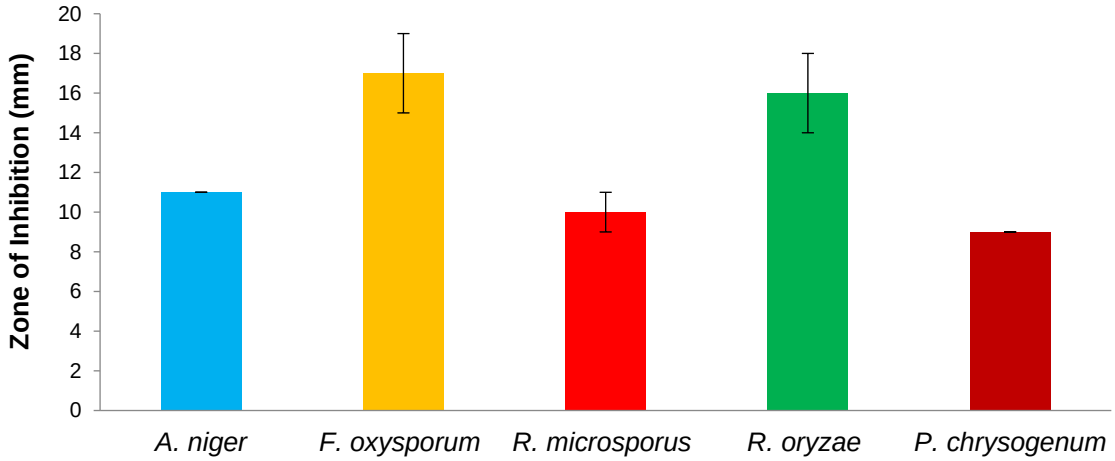

Fig. 7. Antifungal activity of AgNPs against fungal pathogens

Minimum inhibitory concentration

The MIC value of AgNPs was extremely low against both Gram-positive and Gram-negative bacteria in broth dilution technique. The MIC value of AgNPs against bacteria ranged from 12.5 ± 0.25 to 75 ± 2.5 µg/mL. The pathogenic *K. pneumoniae* and *P. aeruginosa* presented the lowest MIC values (12.5 ± 0.25 µg/mL). The drug resistant *S. aureus* strains documented an MIC value of 40 ± 2.5 µg/mL, which was similar to that of

E. faecalis (37.5 ± 1.25 µg/mL). The MIC value was high against the Gram-negative, rod-shaped and facultatively-anaerobic *E. cloacae* (75 ± 2.5 µg/mL) (Fig. 8). The standard streptomycin exhibited lower MIC values than the green synthesized AgNPs. The study by Medina-Cruz *et al*. (2021) showed similar minimum inhibitory concentration (MIC) values of biosynthesized Ag-NPs against *S. aureus*, *B. subtilis*, *E. coli*, *P. aeruginosa*, and *S. typhimurium*, which were found to be 25.0 ppm, 12.5 ppm, 12.5 ppm, 12.5 ppm, and 25.0 ppm, respectively. Correspondingly, the zones of inhibition (ZOIs) were measured at (10.16 ± 0.7) mm, (13.3 ± 0.6) mm, (10.3 ± 0.3) mm, (9.5 ± 0.4) mm, and (9.5 ± 0.4) mm, respectively.

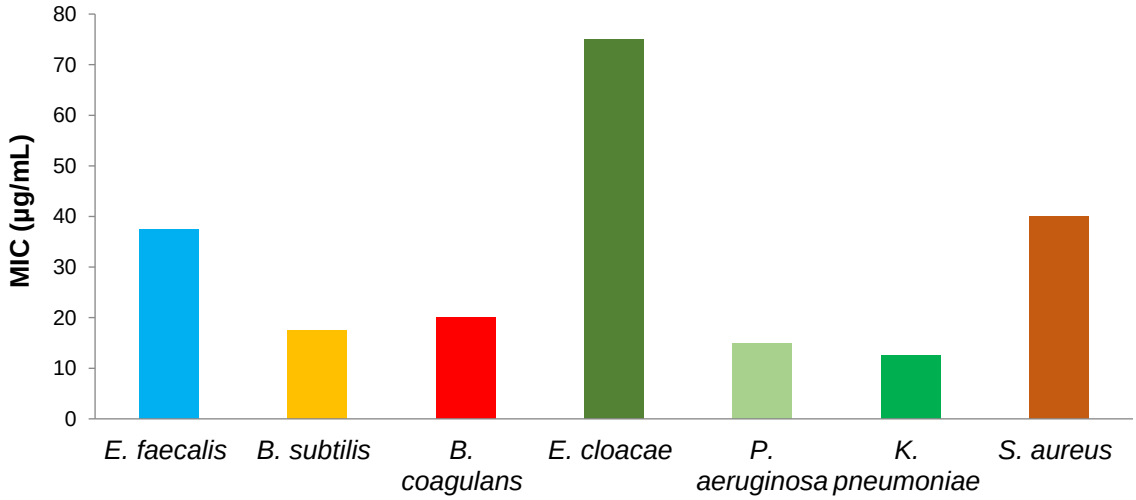

Fig. 8. MIC of AgNPs against bacterial pathogens

Inhibitory effect of fungal biomass

AgNPs inhibited fungal biomass after 5 days of incubation, and the results are depicted in Fig. 9. After 5 days of incubation, AgNPs effectively reduced the fungal biomass in *F. oxysporum* (83 ± 3.1%) and *R. oryzae* (78 ± 2.4%). Moreover, AgNPs showed less biomass inhibitory effect against *A. niger*, *R. microspores*, and *P. chrysogenum*.

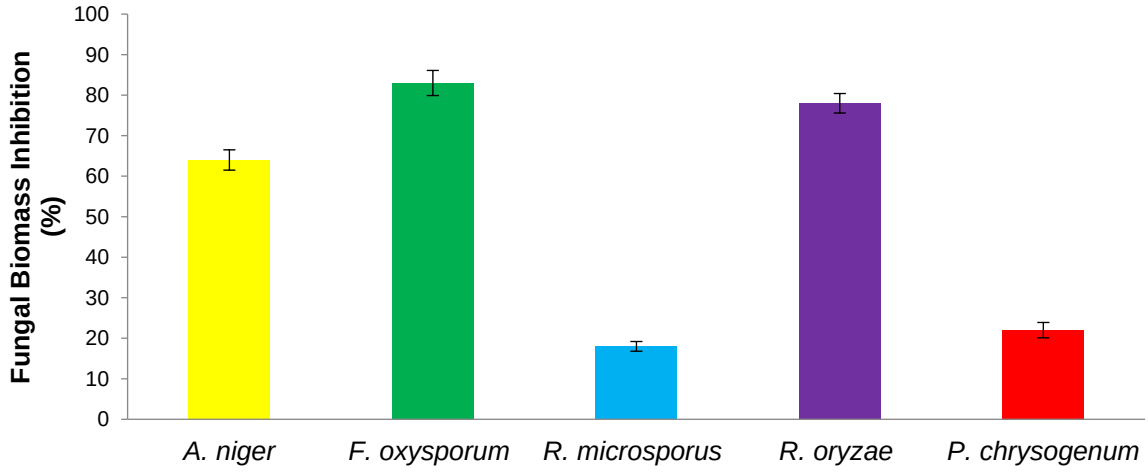

Fig. 9. Fungal biomass inhibitory effect of AgNPs

Antibiofilm activity

The antibiofilm activity of AgNPs was evaluated at various concentrations against *P. aeruginosa* and *K. pneumoniae*, and the results are depicted in Fig. 10. At 1/2 MIC, antibiofilm activity was higher against *K. pneumoniae* (87.4 ± 5.3%) than *P. aeruginosa* (86.1 ± 4.1%). At low AgNPs concentrations, a reduction in antibiofilm activity was observed with respect to the positive control. The synthesized AgNPs showed antibiofilm activity too against *K. pneumoniae* and *P. aeruginosa*. The antibiofilm property was described previously (Shehabeldine *et al*. 2022).

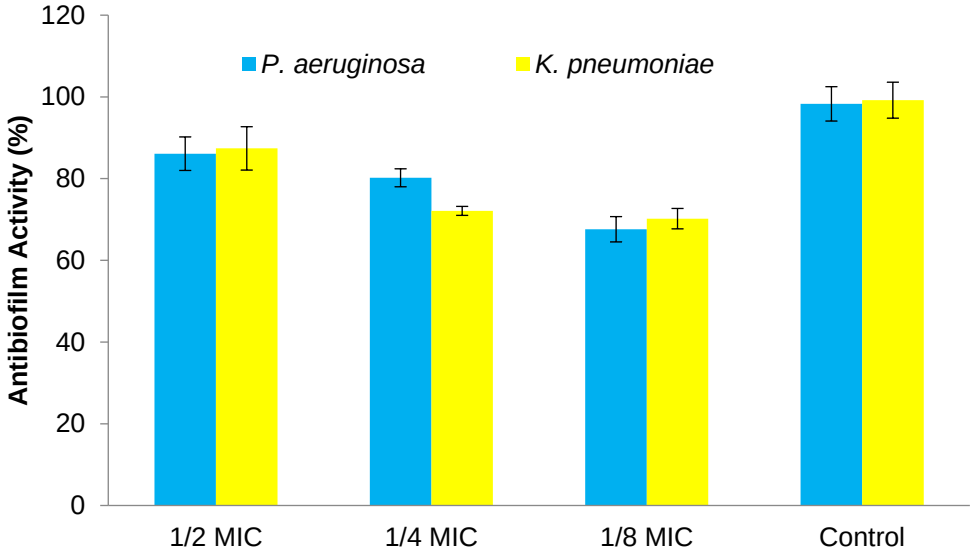

Fig. 10. Antibiofilm activity of AgNPs against *P. aeruginosa* and *K. pneumoniae* at 1/2, 1/4, and 1/8 MIC-values

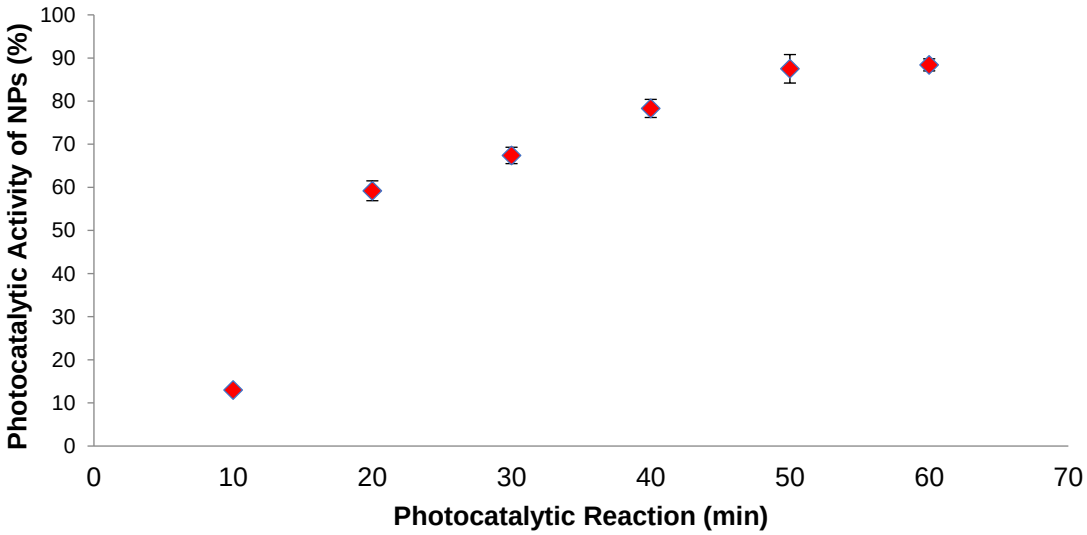

Fig. 11. Photocatalytic activity of AgNPs at various catalytic reaction times. The initial MB dye concentration was 10 ppm, and the photocatalytic reaction was carried out for 60 min.

Photocatalytic activity of AgNPs

The photocatalytic activity of AgNPs was determined using MB dye, and the result is illustrated in Fig. 11. The photocatalytic activity showed a decreased absorbance spectrum in the visible region. The increase in exposure time decreased the absorbance at 660 nm. The percentage MB dye degradation potential was calculated as 13 ± 0.5% degradation after a 10-min photocatalytic reaction. The photocatalytic activity increased with the increased reaction time, and 88.4 ± 1.4% degradation was achieved after 60 min.

Larvicidal activity of AgNPs

The mortality percentage (%) of *Ae. aegypti* exposed to different concentrations of AgNPs after 24 and 48 h is shown in Fig. 12. The concentration of the AgNPs and treatment time affected the larvicidal properties. The mortality of larvae increased after 48 h of exposure compared to 24 h. Likewise, increased mortality was observed at a concentration of 10 mg/L of AgNPs, as compared to 2.5 mg/L. Amarasinghe *et al*. (2020) conducted a study in which they found that silver nanoparticles synthesized through the use of *Annona squamosa* leaf broth exhibited a notable increase in mortality rates among fourth instar larvae of *Aedes aegypti*, commonly known as the yellow fever mosquito.

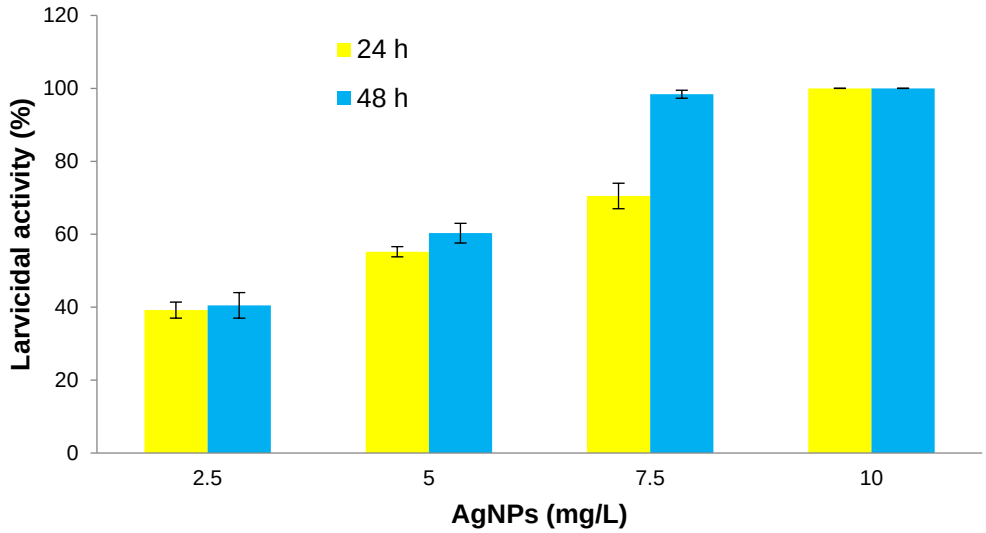

Fig. 12. Larvicidal activity of AgNPs at various concentrations after 24 and 48 h

COD and bacterial load reduction

Municipal wastewater treated with AgNPs reduced the COD, and the result is depicted in Fig. 13a. At 2.5 ppm concentration of AgNPs, the COD reduction was obtained as 55.1 ± 2.1%, but the COD reduction percentage increased at 10 ppm concentration of AgNPs in the wastewater (63.8 ± 1.5%). In contrast, the bacterial population in AgNPs-treated wastewater was estimated as 9700 ± 178 CFU/mL, 5350 ± 102 CFU/mL, 3874 ± 79 CFU/mL, and 3280 ± 22 CFU/mL, at 2.5, 5, 7.5, and 10 ppm concentration of AgNPs, correspondingly (Fig. 13b). The AgNPs exhibited larvicidal activity against *Ae. aegypti*. This experimental evidence demonstrated the multifunctional properties of the synthesized AgNPs. In addition to this, AgNPs were used to treat wastewater, and COD removal potential was registered. The bactericidal activity of AgNPs reduced the bacterial load in the AgNP-treated wastewater (El-Telbany and El-Sharaki 2022). To fully grasp and

harness the multifunctional potential of *A. purpurata*, additional research and clinical investigations are needed.

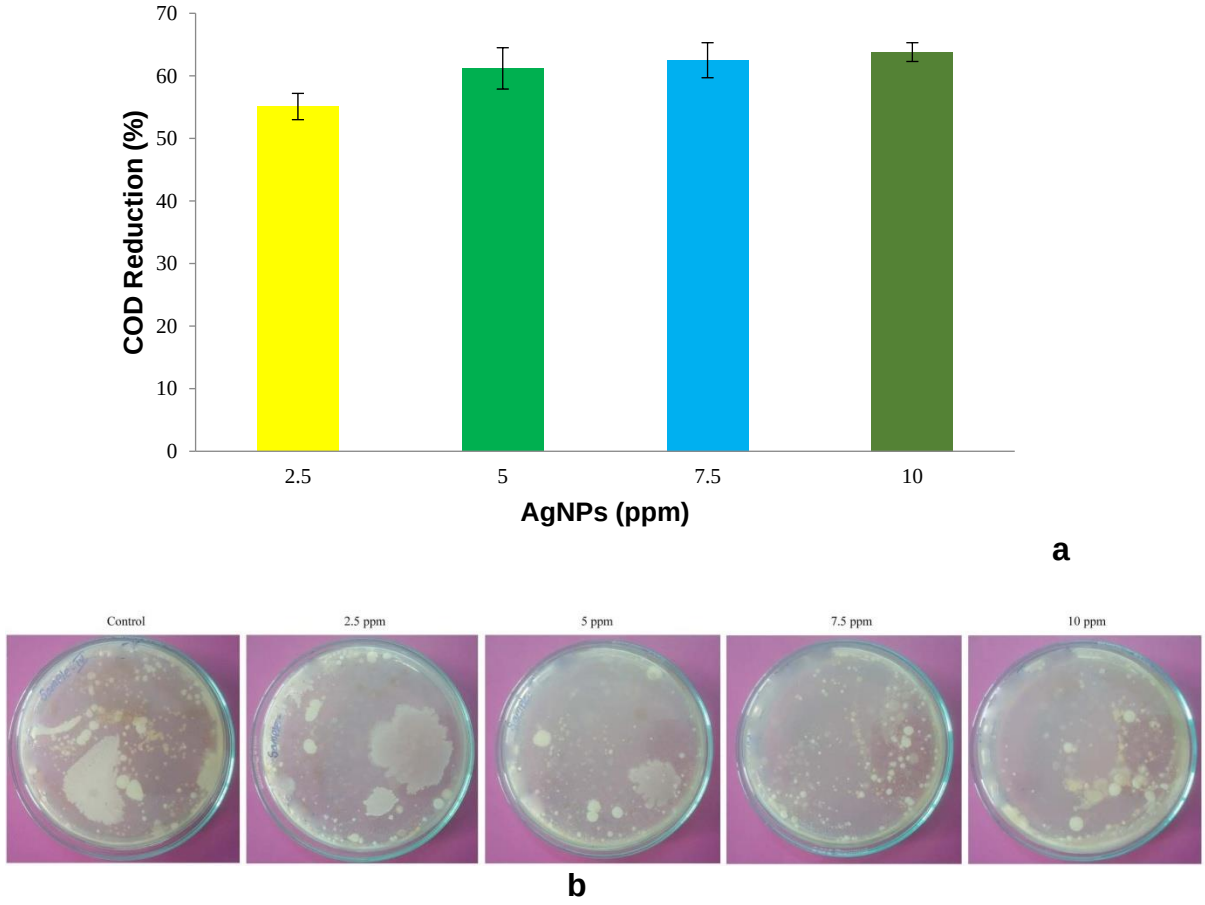

Fig. 13. Reduction of chemical oxygen demand (a) and bacterial population (b) in AgNP (2.5 to 10 ppm)-treated municipal wastewater

CONCLUSIONS

1. Silver nanoparticles were successfully synthesized using leaf extract of *A. purpurata* and characterized using various techniques.
2. Characterization of nanoparticles showed particle sizes ranging from 10 to 30 nm and the presence of silver atoms.
3. The study showed that biologically synthesized silver nanoparticles (AgNPs) using *A. purpurata* leaves possess promising antiproliferative activity in cancer cells, potentially achieved through the induction of apoptosis by activating Caspase 3, with IC50 values of 4.59 ± 0.6 µg/mL in A549 Cells and 3.48 ± 0.4 µg/mL in PA1 cells.
4. The synthesized AgNPs exhibited antimicrobial activities against bacterial and fungal pathogens. The synthesized AgNPs exhibited potent photocatalytic, larvicidal, and COD reduction potentials.

5. However, further research is essential to illuminate the multifunctional properties of *A. purpurata* leaves-based AgNPs *in vivo*.

FUTURE PERSPECTIVES

In the future, the authors' medical research activities are geared towards transforming cancer treatment methodologies with innovative approaches. One such new strategy involves employing aerosol-based nanoparticle therapy to combat lung cancer. By connecting the distinctive characteristics of nanoparticles, the goal is to craft targeted delivery systems practiced on cancerous cells within the lungs, all while mitigating systemic side effects. Also, research is being conducted on the intra-tumoral liposome-mediated nanoparticle delivery, specifically for the treatment of ovarian cancer. Liposomes, characterized as lipid-based vesicles, serve as efficient vehicles for transporting therapeutic agents directly to tumor sites. Through this intensive effort, the aim is to strengthen treatment efficacy while minimizing adverse effects on healthy tissues. In future antimicrobial and biofilm management in medical devices holds immense potential for enhancing patient safety, decrease healthcare-associated infections, and expanding the overall efficacy of medical interventions.

ABBREVIATIONS

1. AgNPs - Silver nanoparticles
2. HCl - Hydrochloric acid
3. H_2SO_4 - Sulphuric acid
4. $FeCl_3$ - Ferric chloride
5. UV-Vis - Ultraviolet-visible
6. FT-IR - Fourier transform infrared
7. HR-TEM - High-resolution transmission electron microscopy
8. EDX - Energy dispersive microanalysis
9. MTT - 3-(4,5-dimethyl-2-thiazolyl)-2,5-diphenyl-tetrazolium bromide
10. DMSO - Dimethyl sulfoxide
11. PBS - Phosphate-buffered saline
12. MHB - Mueller Hinton broth
13. CFU - Colony forming unit
14. MB - Methylene blue
15. COD - Chemical oxygen demand
16. PA1 - ovarian cancer cell line
17. A549 - Lung cancer cell line

ACKNOWLEDGMENTS

Researchers Supporting Project number (RSP2024R414), King Saud University, Riyadh, Saudi Arabia.

Conflict of interest

The authors declare no competing interests.

REFERENCES CITED

Abdulazeem, L., Alasmari, A. F., Alharbi, M., Alshammari, A., and Muhseen, Z. T. (2023). "Utilization of aqueous broccoli florets extract for green synthesis and characterization of silver nanoparticles, with potential biological applications," *Heliyon* 9(9), article ID e19723. DOI: 10.1016/j.heliyon.2023.e19723

Aboyewa, J. A., Sibuyi, N. R. S., Meyer, M., and Oguntibeju, O. O. (2021). "Green synthesis of metallic nanoparticles using some selected medicinal plants from southern Africa and their biological applications," *Plants* 10(9), article 1929. DOI: 10.3390/plants10091929

Adhya, D., Annuario, E., Lancaster, M. A., Price, J., Baron-Cohen, S., and Srivastava, D. P. (2018). "Understanding the role of steroids in typical and atypical brain development: Advantages of using a 'brain in a dish' approach," *Journal of Neuroendocrinology* 30(2), article 12547. DOI: 10.1111/jne.12547

Al-Wrafy, F. A., Al-Gheethi, A., Ponnusamy, S. K., Noman, E. A., and Fattah, S. A. (2022). "Nanoparticles approach to eradicate bacterial biofilm-related infections: A critical review," *Chemosphere* 288, article ID 132603. DOI: 10.1016/j.chemosphere.2021.132603

Amarasinghe, L. D., Wickramarachchi, P. A. S. R., Aberathna, A. a. a. U., Sithara, W. S., and De Silva, C. R. (2020). "Comparative study on larvicidal activity of green synthesized silver nanoparticles and *Annona glabra* (Annonaceae) aqueous extract to control *Aedes aegypti* and *Aedes albopictus* (Diptera: Culicidae)," *Heliyon* 6(6), article e04322. DOI: 10.1016/j.heliyon.2020.e04322

Anandalakshmi, K., Venugobal, J., and Ramasamy, V. (2015). "Characterization of silver nanoparticles by green synthesis method using *Pedalium murex* leaf extract and their antibacterial activity," *Applied Nanoscience* 6(3), 399-408. DOI: 10.1007/s13204-015-0449-z

Anjum, S., Ishaque, S., Fatima, H., Farooq, W., Hano, C., Abbasi, B. H., and Anjum, I. (2021). "Emerging applications of nanotechnology in healthcare systems: Grand challenges and perspectives," *Pharmaceuticals* 14(8), article 707. DOI: 10.3390/ph14080707

Anusooriya, P., Kannappan, P., and Gopalakrishnan, V. K. (2022). "Anticancer activity of *Alpinia purpurata* (Vieill) K. Schum. against MNU and testosterone induced prostate cancer in male Wistar albino rats," *Pharmacological Research - Modern Chinese Medicine* 3, article ID 100105. DOI: 10.1016/j.prmcm.2022.100105

Artiukh, L., Povnitsa, O., Zahorodnia, S., Pop, C. V., and Rizun, N. (2022). "Effect of coated silver nanoparticles on cancerous *vs.* healthy cells," *Journal of Toxicology* 2022, article ID 1519104. DOI: 10.1155/2022/1519104

Arul Raj, C., Sophia, D., Ragavendran, P., Starlin, T., Ma, R., and Gopalakrishnan, V. K. (2012). "Leaf extract of *Alpinia purpurata* (Vieill.) K. Schum screened for its phytochemical constituents and antibacterial and anticancer activities," *Journal of Chinese Integrative Medicine* 10(12), 1460-1464. DOI: 10.3736/jcim20121219

Baharara, J., Namvar, F., Ramezani, T., Mousavi, M., and Mohamad, R. (2015). "Silver nanoparticles biosynthesized using *Achillea biebersteinii* flower extract: Apoptosis induction in MCF-7 cells *via* caspase activation and regulation of Bax and Bcl-2 gene expression," *Molecules* 20(2), 2693-2706. DOI: 10.3390/molecules20022693

Castro-Puyana, M., Marina, M. L., and Plaza, M. (2017). "Water as green extraction solvent: Principles and reasons for its use," *Current Opinion in Green and Sustainable Chemistry*, 5, 31-36. DOI: 10.1016/j.cogsc.2017.03.009

Chaturvedi, V. K., Yadav, N., Neeraj, K., Ellah, N. H. A., Bohara, R. A., Rehan, I. F., Marraiki, N., Batiha, G. E., Hetta, H. F., and Singh, M. (2020). "*Pleurotus sajor-caju*-Mediated synthesis of silver and gold nanoparticles active against colon cancer cell lines: A new era of herbonanoceutics," *Molecules* 25(13), article 3091. DOI: 10.3390/molecules25133091

De Macedo, E. F., Santos, N. S., Nascimento, L. S., Mathey, R., Brenet, S., De Moura, M. S., Hou, Y., and Tada, D. B. (2022). "Interaction between nanoparticles, membranes and proteins: A surface plasmon resonance study," *International Journal of Molecular Sciences* 24(1), article 591. DOI: 10.3390/ijms24010591

El-Telbany, M., and El-Sharaki, A. (2022). "Antibacterial and anti-biofilm activity of silver nanoparticles on multi-drug resistance *Pseudomonas aeruginosa* isolated from dental-implant," *Journal of Oral Biology and Craniofacial Research* 12(1), 199-203. DOI: 10.1016/j.jobcr.2021.12.002

Gad, S. S., Abdelrahim, D. S., Ismail, S. H., and Ibrahim, S. M. (2021). "Selenium and silver nanoparticles: A new approach for treatment of bacterial and viral hepatic infections *via* modulating oxidative stress and DNA fragmentation," *Journal of Biochemical and Molecular Toxicology* 36(3), article ID 22972. DOI: 10.1002/jbt.22972

Gurunathan, S., Han, J. S., Eppakayala, V., Jeyaraj, M., and Kim, J. (2013). "Cytotoxicity of biologically synthesized silver nanoparticles in MDA-MB-231 human breast cancer cells," *BioMed Research International* 2013, 1-10. DOI: 10.1155/2013/535796

Hashem, S., Ali, T., Akhtar, S., Nisar, S., Sageena, G., Ali, S., Al-Mannai, S., Therachiyil, L., Mir, R., Elfaki, I., *et al.* (2022). "Targeting cancer signaling pathways by natural products: Exploring promising anti-cancer agents," *Biomedicine & Pharmacotherapy* 150, article ID 113054. DOI: 10.1016/j.biopha.2022.113054

Huang, J., Chan, W. C., Ngai, C. H., Lok, V., Zhang, L., Lucero-Prisno, D. E., III, Xu, W., Zheng, Z. J., Elcarte, E., Withers, M., Wong, M. C. S., and on behalf of NCD Global Health Research Group of Association of Pacific Rim Universities (APRU) (2022). "Worldwide burden, risk factors, and temporal trends of ovarian cancer: A global study," *Cancers* 14(9), article 2230. DOI: 10.3390/cancers14092230

Khan, H., Alam, W., Alsharif, K. F., Aschner, M., Pervez, S., and Saso, L. (2022). "Alkaloids and colon cancer: Molecular mechanisms and therapeutic implications for cell cycle arrest," *Molecules* 27(3), article 920. DOI: 10.3390/molecules27030920

Kumar, D. G., Achar, R. R., Kumar, J. R., George, A., Gopalakrishnan, V., Pradeep, S., Shati, A. A., Alfaifi, M. Y., Elbehairi, S. E. I., Silina, E., *et al.* (2023). "Assessment of antimicrobial and anthelmintic activity of silver nanoparticles bio-synthesized from *Viscum orientale* leaf extract," *BMC Complementary Medicine and Therapies* 23(1), article 167. DOI: 10.1186/s12906-023-03982-1

Li, X., Wang, Y. Y., Huang, J., Chen, C. Y., Wang, Z., and Xie, H. (2020). "Silver nanoparticles: Synthesis, medical applications and biosafety," *Theranostics* 10(20), 8996-9031. DOI: 10.7150/thno.45413

Lee, Y. S., Kim, D. H., Lee, Y. H., Oh, J. H., Yoon, S., Choi, M. S., Lee, S. K., Kim, J. W., Lee, K., and Song, C. (2011). "Silver nanoparticles induce apoptosis and G2/M arrest via PKCζ-dependent signaling in A549 lung cells," *Archives of Toxicology* 85(12), 1529-1540. DOI: 10.1007/s00204-011-0714-1

Mathur, P., Sathishkumar, K., Chaturvedi, M., Das, P., and Stephen, S. (2023). "Cancer incidence estimates for 2022 & projection for 2025: Result from National Cancer Registry Programme, India," *Indian Journal of Medical Research* 156(4&5), 598-607. DOI: 10.4103/ijmr.ijmr_1821_22

Mittal, A. K., Chisti, Y., and Banerjee, U. C. (2013). "Synthesis of metallic nanoparticles using plant extracts," *Biotechnology Advances* 31(2), 346-356. DOI: 10.1016/j.biotechadv.2013.01.003

Medina-Cruz, D., Vernet-Crua, A., Mostafavi, E., González, M. U., Martínez, L., Jones, A.-A. D., Kusper, M., Sotelo, E., Gao, M., Geoffrion, L. D., Shah, V., Guisbiers, G., Cholula-Díaz, J. L., Guillermier, C., Khanom, F., Huttel, Y., García-Martín, J. M., and Webster, T. J. (2021). "Aloe vera-mediated TE nanostructures: Highly potent antibacterial agents and moderated anticancer effects," *Nanomaterials* 11(2), article 514. DOI: 10.3390/nano11020514

Mohammadi, M., Zaki, L., KarimiPourSaryazdi, A., Tavakoli, P., Tavajjohi, A., Poursalehi, R., Delavari, H., and Ghaffarifar, F. (2021). "Efficacy of green synthesized silver nanoparticles *via* ginger rhizome extract against *Leishmania major in vitro*," *PLOS ONE* 16(8), article ID e0255571. DOI: 10.1371/journal.pone.0255571

Mejía-Mendez, J. L., Lopez-Mena, E. R., and Sanchez-Arreola, E. (2023). "Activities against lung cancer of biosynthesized silver nanoparticles: A review," *Biomedicines* 11(2), article 389. DOI: 10.3390/biomedicines11020389

Mosmann, T. R. (1983). "Rapid colorimetric assay for cellular growth and survival: Application to proliferation and cytotoxicity assays," *Journal of Immunological Methods* 65(1–2), 55-63. DOI: 10.1016/0022-1759(83)90303-4

Mourdikoudis, S., Pallares, R. M., and Thanh, N. T. K. (2018). "Characterization techniques for nanoparticles: comparison and complementarity upon studying nanoparticle properties," *Nanoscale* 10(27), 12871-12934. DOI: 10.1039/c8nr02278j

Plotnikov, E., Tretayakova, M. S., Garibo-Ruíz, D., Rodríguez-Hernández, A. G., Pestryakov, A., Toledano-Magaña, Y., and Bogdanchikova, N. (2023). "A comparative study of cancer cells susceptibility to silver nanoparticles produced by electron beam," *Pharmaceutics* 15(3), article 962. DOI: 10.3390/pharmaceutics15030962

Rezazadeh, M., Davatsaz, Z., Emami, J., Hasanzadeh, F., and Jahanian-Najafabadi, A. (2018). "Preparation and characterization of spray-dried inhalable powders containing polymeric micelles for pulmonary delivery of paclitaxel in lung cancer," *Journal of Pharmacy and Pharmaceutical Sciences* 21(1s), 200s-214s. DOI: 10.18433/jpps30048

Sakr, T. M., Khowessah, O. M., Motaleb, M. A., El-Bary, A. A., El-Kolaly, M. T., and Swidan, M. M. (2018). "I-131 doping of silver nanoparticles platform for tumor theranosis guided drug delivery," *European Journal of Pharmaceutical Sciences* 122, 239-245. DOI: 10.1016/j.ejps.2018.06.029

Shehabeldine, A. M., Salem, S. S., Ali, O. M., Abd-Elsalam, K. A., Elkady, F. M., and Hashem, A. H. (2022). "Multifunctional silver nanoparticles based on chitosan: Antibacterial, antibiofilm, antifungal, antioxidant, and wound-healing activities," *Journal of Fungi* 8(6), article 612. DOI: 10.3390/jof8060612

Takáč, P., Michalková, R., Čižmáriková, M., Bedlovičová, Z., Balážová, Ľ., and Takáčová, G. (2023). "The role of silver nanoparticles in the diagnosis and treatment

of cancer: are there any perspectives for the future?," *Life* 13(2), article 466. DOI: 10.3390/life13020466

Thotathil, V., Rizk, H. H., Fakrooh, A., and Sreerama, L. (2022). "Phytochemical analysis of *Acacia ehrenbergiana* (Hayne) grown in Qatar: Identification of active ingredients and their biological activities," *Molecules* 27(19), article 6400. DOI: 10.3390/molecules27196400

Ullah, A., Munir, S., Badshah, S. L., Khan, N., Ghani, L., Jaremko, M., and Emwas, A. (2020). "Important flavonoids and their role as a therapeutic agent," *Molecules* 25(22), article 5243. DOI: 10.3390/molecules25225243

Vijay, R., Drisya, V. M., Selta, D. R. F., Rathi, M. A., Krishnan, Vk. G., Alkhalifah, D. H. M., and Hozzein, W. N. (2023). "Synthesis and characterization of silver nanomaterial from aqueous extract of *Commelina forskaolii* and its potential antimicrobial activity against Gram negative pathogens," *Journal of King Saud University - Science* 35(1), article ID 102373. DOI: 10.1016/j.jksus.2022.102373

Zhou, M., Liu, X., Li, Z., Huang, Q., Li, F., and Li, C. Y. (2018). "Caspase-3 regulates the migration, invasion and metastasis of colon cancer cells," *International Journal of Cancer* 143(4), 921-930. DOI: 10.1002/ijc.31374

Zuhrotun, A., Oktaviani, D. J., and Hasanah, A. N. (2023). "Biosynthesis of gold and silver nanoparticles using phytochemical compounds," *Molecules* 28(7), article 3240. DOI: 10.3390/molecules28073240

Article submitted: January 25, 2024; Peer review completed: March 22, 2024; Revised version received and accepted: April 3, 2024; Published: April 12, 2024.
DOI: 10.15376/biores.19.2.3328-3352